Inorg. Chem. **2002**, *41*, 4206–4210

High-Temperature, High-Pressure Hydrothermal Synthesis, Crystal Structure, and Solid State NMR Spectroscopy of a New Vanadium(IV) Silicate: $Rb_2(VO)(Si_4O_{10})\cdot xH_2O$

Chun-Yi Li,[†] Chan-Yen Hsieh,[†] Hsiu-Mei Lin,[‡] Hsien-Ming Kao,[†] and Kwang-Hwa Lii*[,†,‡]

Department of Chemistry, National Central University, Chungli, and Institute of Chemistry, Academia Sinica, Taipei, Taiwan, R.O.C.

Received March 8, 2002

A new vanadium(IV) silicate, $Rb_2(VO)(Si_4O_{10})\cdot xH_2O$ ($x \approx 0.1$), has been synthesized by a high-temperature, high-pressure hydrothermal method. It crystallizes in the tetragonal space group $I4_1md$ (No. 109) with $a = 12.2225(7)$ Å, $c = 7.7948(6)$ Å, and $Z = 4$. The structure consists of spiral chains of corner-sharing SiO_4 tetrahedra linked to neighboring chains via corner sharing to form a 3-D silicate framework which delimits channels to accommodate the VO^{2+} groups. The Rb^+ ions are located in the cavities within the silicate framework. Magnetic susceptibility confirms the valence of vanadium. A partially occupied lattice water site is confirmed by IR and solid state ^1H NMR spectroscopy. The structure of the title compound is considerably different from those of the synthetic silicate $K_2(VO)(Si_4O_{10})\cdot H_2O$ and the two polymorphs of the natural mineral $Ca(VO)(Si_4O_{10})\cdot 4H_2O$, although they have identical framework stoichiometry.

Introduction

Organically templated transition metal phosphates have been extensively studied in recent years because of interesting structural chemistry and potential applications in catalysis.[1−3] Many of these metal phosphates have open framework structures. The empty space in the structure is often filled with organic cations. However, in most cases, the organic templates cannot be removed without collapse of the frameworks. Few organically templated metal phosphates have sufficient thermal stability to be used in commercial processes. This is in contrast to the high thermal stability and extensive application of zeolites in refinery and petrochemical processes. Therefore, studies have been directed to the synthesis of transition metal silicates to produce more stable frameworks. The microporous titanosilicate ETS-10 is a well-known example.[4,5] The first large-pore vanadosilicate called AM-6 possessing a structure similar to that of ETS-10 has also been reported.[6] Although vanadium has already been introduced into the frameworks of certain zeolites in small amounts, few microporous framework vanadosilicates are known to contain stoichiometric amounts of vanadium. Recently, Jacobson et al. reported two vanadosilicates, $K_2(VO)(Si_4O_{10})\cdot H_2O$ and $Cs_2(VO)(Si_6O_{14})\cdot 3H_2O$, which have small pore frameworks.[7] They were synthesized under mild hydrothermal conditions in a Teflon-lined autoclave. Other synthetic vanadosilicates include synthetic haradaite $SrVSi_2O_7$,[8] β-$BaVSi_2O_7$,[9] $Ln_4V_5Si_4O_{22}$ ($Ln_4 = La_{3.4}Ca_{0.6}$, La_4, Pr_4, Nd_4),[10−13] and $NaVSi_2O_6$.[14] All of them were synthesized by solid-state reactions. Vanadium silicates are

* To whom correspondence should be addressed. E-mail: liikh@cc.ncu.edu.tw.
[†] National Central University.
[‡] Academia Sinica.

(1) Haushalter, R. C.; Mundi, L. A. *Chem. Mater.* **1992**, *4*, 31 and references therein.
(2) Lii, K.-H.; Huang, Y.-F.; Zima, V.; Huang, C.-Y.; Lin, H.-M.; Jiang, Y.-C.; Liao, F.-L.; Wang, S.-L. *Chem. Mater.* **1998**, *10*, 2599 and references therein.
(3) Cheetham, A. K.; Ferey, G.; Loiseau, T. *Angew. Chem., Int. Ed.* **1999**, *38*, 3268 and references therein.
(4) Kuznicki, S. M. U.S. Patent 4 853 202, 1989.
(5) Rocha, J.; Anderson, M. W. *Eur. J. Inorg. Chem.* **2000**, 801 and references therein.
(6) Rocha, J.; Brandão, P.; Lin, Z.; Anderson, M. W.; Alfredsson, V.; Terasaki, O. *Angew. Chem., Int. Ed. Engl.* **1997**, *36*, 100.
(7) Wang, X.; Liu, L.; Jacobson, A. *Angew. Chem., Int. Ed.* **2001**, *40*, 2174.
(8) Berger, T.; Range, K.-J. *Z. Naturforsch.* **1996**, *B51*, 1099.
(9) Liu, G.; Greedan, J. E. *J. Solid State Chem.* **1994**, *108*, 267.
(10) Chen, S. C.; Ramanujachary, K. V.; Greenblatt, M. *Inorg. Chem.* **1994**, *33*, 5994.
(11) Gueho, C.; Giaquinta, D.; Mansot, J. L.; Ebel, T.; Palvadeau, P. *Chem. Mater.* **1995**, *7*, 486.
(12) Chen, J.; Guo, G.; Zhuang, H.; Huang, J.; Zhang, Q. *J. Solid State Chem.* **1995**, *116*, 211.
(13) Chen, J.; Guo, G.; Zhuang, H.; Huang, J.; Zhang, Q. *Acta Crystallogr.* **1996**, *C52*, 2125.
(14) Ohashi, H.; Osawa, T.; Sato, A. *Acta Crystallogr.* **1994**, *C50*, 1652.

10.1021/ic020187q CCC: $22.00 © 2002 American Chemical Society
Published on Web 07/10/2002

also present as minerals such as cavansite,[15] pentagonite,[15] and haradaite.[16] The former two minerals are dimorphs of $Ca(VO)(Si_4O_{10})\cdot 4H_2O$ and have a framework that can be considered to be based on the same building principles as those for $K_2(VO)(Si_4O_{10})\cdot H_2O$ and $Cs_2(VO)(Si_6O_{14})\cdot 3H_2O$. Because we have been interested in the exploratory synthesis of mixed octahedral−tetrahedral framework oxides, we therefore extended the search for new materials into the system of transition metal silicates. Our synthetic methods are 2-fold, namely mild hydrothermal reactions in Teflon-lined autoclaves at 100−200 °C and high-temperature, high-pressure hydrothermal reactions in gold ampules contained in a high-pressure reaction vessel at 500−600 °C. In this work, we report high-temperature, high-pressure hydrothermal synthesis and characterization of a new vanadosilicate, $Rb_2(VO)(Si_4O_{10})\cdot xH_2O$ ($x \approx 0.1$). It has the same framework stoichiometry as those of $K_2(VO)(Si_4O_{10})\cdot H_2O$ and $Ca(VO)(Si_4O_{10})\cdot 4H_2O$, but it adopts a considerably different structure.

Experimental Section

Synthesis and Characterization. High-temperature, high-pressure hydrothermal synthesis was performed in gold ampules contained in a Leco Tem-Pres autoclave where pressure was provided by water. The degree of filling of the autoclave by water at room temperature is 50%. A reaction mixture of 0.0362 g of VO_2, 0.105 g of SiO_2, and 510 μL of 3 M RbOH(aq) (molar ratio Rb:V:Si = 3.5:1:4) in a 5.7 cm long gold ampule (inside diameter = 0.48 cm) was heated at 550 °C for 3 d. The pressure was estimated to be 110 MPa. The autoclave was then cooled to 250 °C at 5 °C/h and quenched at room temperature by removing the autoclave from the furnace. The product was filtered off, washed with water, rinsed with ethanol, and dried at ambient temperature. The reaction produced 0.041 g of green dipyramidal crystals of $Rb_2(VO)(Si_4O_{10})\cdot xH_2O$ in 19% yield based on vanadium. A qualitative EDX analysis of several green crystals confirmed the presence of Rb, V, and Si. The bulk product was monophasic as indicated by the X-ray powder pattern in Figure 1.

We were unable to confirm the presence of a trace amount of lattice water in the compound using TG analysis, and we therefore turned to IR and NMR spectroscopy. The infrared spectrum was recorded on a Perkin-Elmer Paragon 1000 FT-IR spectrometer using the KBr pellet method. ^{1}H MAS (magic angle spinning) NMR spectra were acquired on a Bruker AVANCE-400 spectrometer using a spin−echo pulse sequence with a $\pi/2$ pulse width of 4 μs and a repetition time of 4 s. The chemical shifts were externally referenced to TMS (tetramethylsilane) at 0.0 ppm.

Variable-temperature magnetic susceptibility $\chi(T)$ data were obtained on 35.8 mg of polycrystalline sample of $Rb_2(VO)(Si_4O_{10})\cdot xH_2O$ from 2 to 300 K in a magnetic field of 5000 G after zero-field cooling using a SQUID magnetometer. Correction for diamagnetism was made according to Selwood.[17]

Single-Crystal X-ray Diffraction. A green crystal of dimensions $0.2 \times 0.2 \times 0.3$ mm^3 was selected for indexing and intensity data collection on a Siemens Smart CCD diffractometer equipped with a normal focus, 3 kW sealed tube X-ray source. Intensity data were collected in 1271 frames with increasing ω (width of 0.3° per frame). The number of observed unique reflections ($F_o > 4\sigma(F_o)$) is 669 ($2\theta_{max} = 56.55°$, $R_{int} = 0.0405$). Empirical absorption corrections based on symmetry equivalents were performed by using SADABS program for Siemens area detector ($T_{max,\ min} = 0.862$, 0.353).[18] On the basis of systematic absences, statistics of intensity distribution, and successful solution and refinement of the structure, the space group was determined to be $I4_1md$ (No. 109). The structure was solved by direct methods: The metal and Si atoms were first located, and the O atoms were found from difference Fourier maps. A few cycles of least squares refinement including the atomic coordinates and anisotropic thermal factors for all atoms converged at R1 = 0.0295, wR2 = 0.0738, and $S = 1.091$. The Flack x parameter was 0.04(1), indicative of a correct absolute structure. At this point, the maximum and minimum residual electron densities ($\Delta\rho_{max,\ min}$) in difference Fourier maps were 1.59 and −0.76 e·Å^{-3}, respectively. The largest residual density is at (0, 0, −0.6679) and is presumably attributed to a lattice water site with partial occupancy. This water site is at a distance of 2.89 Å from the vanadium atom and refined to a site occupancy factor of 0.029(6) with a fixed isotropic thermal parameter ($U = 0.5$ Å^2), which is approximately equivalent to 0.1 water molecule per formula unit. The presence of a lattice water molecule was confirmed by IR and ^{1}H MAS NMR spectroscopy. The final cycles of least squares refinement converged at R1 = 0.0286, wR2 = 0.0723, and $S = 1.133$. $\Delta\rho_{max,\ min} = 0.94$, −0.72 e·Å^{-3}. Neutral-atom scattering factors were used for all the atoms. Anomalous dispersion and secondary extinction corrections were applied. All calculations were carried out with the PC version of the SHELXTL program package. The crystallographic data are given in Table 1,

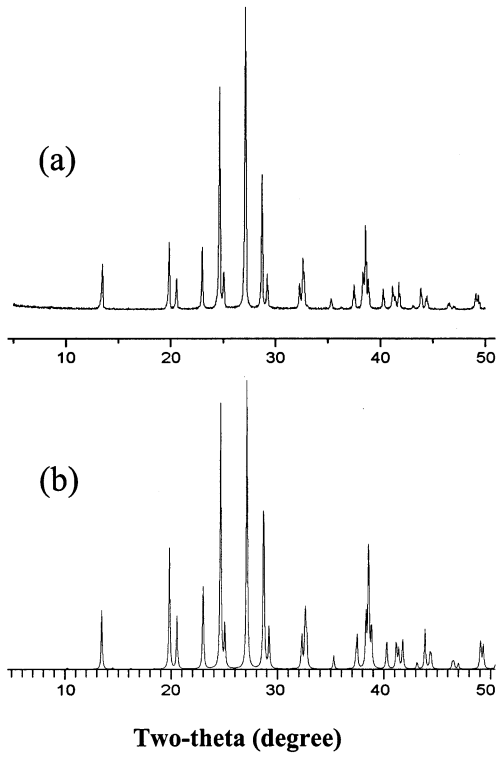

Figure 1. (a) X-ray powder pattern of $Rb_2(VO)(Si_4O_{10})\cdot xH_2O$. (b) Simulated powder pattern from the atomic coordinates derived from single-crystal X-ray diffraction.

(15) Evans, H. T., Jr. *Am. Mineral.* **1973**, *58*, 412.
(16) Takeuchi, Y.; Joswig, W. *Mineral. J.* **1967**, *5*, 98.
(17) Selwood, P. W. *Magnetochemistry*; Interscience: New York, 1956.
(18) Sheldrick, G. M. *SADABS Program*; Siemens Analytical X-ray Instrument Division: Madison, WI, 1998.

Table 1. Crystallographic Data for $Rb_2(VO)(Si_4O_{10})\cdot xH_2O$ ($x \approx 0.1$)

empirical formula	$O_{11}Rb_2Si_4V$
fw	510.24
color	green
size, mm^3	$0.2 \times 0.2 \times 0.3$
cryst syst	tetragonal
space group	$I4_1md$ (No. 109)
a/Å	12.2225(7)
c/Å	7.7948(6)
V/Å^3	1164.5(3)
Z	4
D_{calcd}, g·cm^{-3}	2.910
T, °C	23
λ(Mo Kα), Å	0.71073
μ(Mo Kα), cm^{-1}	96.2
$T_{min, max}$	0.353, 0.862
no. unique data [$I > 2\sigma(I)$]	669
no. variables	51
R1,[a] wR2[b]	0.0286 (0.0292), 0.0723

[a] $R1 = \sum||F_o| - |F_c||/\sum|F_o|$. The value in parentheses is for all 686 data. [b] $wR2 = [\sum w(F_o^2 - F_c^2)^2/\sum w(F_o^2)^2]^{1/2}$, $w = 1/[\sigma^2(F_o^2) + (aP)^2 + bP]$, $P = [\max(F_o, 0) + 2(F_c)^2]/3$, where $a = 0.0469$ and $b = 1.90$.

Table 2. Atomic Coordinates for $Rb_2(VO)(Si_4O_{10})\cdot xH_2O$ ($x \approx 0.1$)

atom	x	y	z	U_{eq}[a]
Rb	0	0.21221(5)	0.05787(7)	0.0283(2)
V	0	0	−0.2972(2)	0.0119(3)
Si	0.29137(8)	0.11965(8)	0.2654(1)	0.0107(2)
O(1)	0.2515(4)	0	0.1978(6)	0.0182(8)
O(2)	0.1841(3)	0.1812(3)	0.3393(5)	0.0261(7)
O(3)	0.3897(3)	0.1120(3)	0.3966(5)	0.0249(8)
O(4)	0	0	−0.091(1)	0.029(2)
Ow[b]	0	0	0.34(1)	0.05

[a] U_{eq} is defined as one-third of the trace of the orthogonalized U_{ij} tensor. [b] The site occupancy factor of Ow is 0.029(6).

Table 3. Bond Lengths (Å) and Bond Valence Sums (∑s) for $Rb_2(VO)(Si_4O_{10})\cdot xH_2O$ ($x \approx 0.1$)

Rb−O(1)	3.071(5)	Rb−O(2)	3.166(4) (2×)
Rb−O(3)	2.831(3) (2×)	Rb−O(4)	2.843(3)
∑s (Rb−O) = 0.93			
V−O(3)	1.971(3) (4×)	V−O(4)	1.604(8)
∑s (V−O) = 4.04			
Si−O(1)	1.629(2)	Si−O(2)	1.618(3)
Si−O(2)^{i}[a]	1.618(4)	Si−O(3)	1.581(3)
∑s (Si−O) = 4.14			

[a] Symmetry code: (i) $-y + {}^1/_2$, x, $z - {}^1/_4$.

the atomic coordinates are in Table 2, and bond lengths and bond valence sums are in Table 3.[19]

Results and Discussion

$Rb_2(VO)(Si_4O_{10})\cdot xH_2O$ crystallizes in the polar tetragonal space group $I4_1md$. The asymmetric unit consists of 7 unique atoms. The V atom and the vanadyl oxygen atom O(4) are at 4a special positions with 2*mm* point symmetry. The Rb atom and O(1) are at 8b special positions, and on the mirror plane at $x = 0$. All other atoms are at general positions. As shown in Figure 2, the structure is constructed from the following structural elements: SiO_4 tetrahedra, each with three corners shared with other tetrahedra, and the fourth corner coordinated to one V atom and one Rb atom; VO^{2+} groups coordinated to apexes of 4 SiO_4 tetrahedra so that V is in square-pyramidal coordination with O atoms; Rb^+ ions in 6-fold coordination with O atoms; and partially occupied

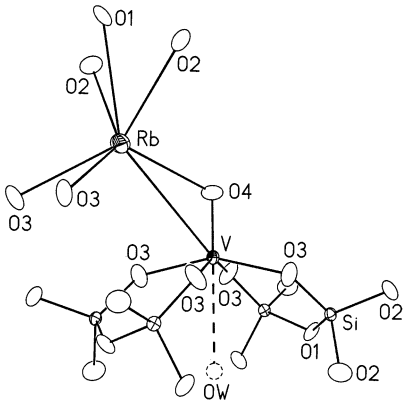

Figure 2. Building units of $Rb_2(VO)(Si_4O_{10})\cdot xH_2O$ showing atom labeling scheme. Thermal ellipsoids are shown at 50% probability. The lattice water oxygen atom is shown in dotted circle.

water molecules. The coordination number of the Rb^+ cation was determined on the basis of the maximum gap in the Rb−O distances. The maximum cation−anion distance, L_{max}, according to Donnay and Allmann was also considered (L_{max} = 3.42 Å for Rb−O).[20] Therefore, the Rb^+ cation is coordinated by six oxygen atoms with the seventh Rb−O distance at 3.604 Å. The valence sum of the six Rb−O bonds is 0.93. The Si−O bond lengths have an average value of 1.611 Å in good agreement with the expected value of 1.609 Å predicted by Brown and Gibbs for silicate structures with the average coordination number for silicate oxygen ⟨CN-(O)⟩ = 2.[21] The Si−O_{br} bonds between silicon and an oxygen atom O_{br} linking two Si atoms are considerably longer than the Si−O_{term} bond between silicon and the terminal oxygen atom O(3) linked to only one silicon atom (average bond lengths are 1.621 and 1.581 Å, respectively). The tetrahedral angles do show reduced basal angles and enlarged apical angles (average values are 104.7° and 113.9°, respectively). The vanadium atom is in the square-pyramidal coordination typical of the tetravalent state, with an apical V−O bond length of 1.606 Å and four basal bond lengths of 1.971 Å. Bond valence sum calculation confirms the tetravalent state for the vanadium atom. A water molecule with a site occupancy factor of 0.029(6) is trans to the vanadyl oxygen and 2.89 Å from vanadium, encroaching on the coordination sphere. The hydrogen bonds between the water molecule and neighboring oxygen atoms are very weak, as indicated by the very long O···O distances (>3.0 Å). The IR spectrum shows sharp bands of the stretching and bending modes of the water molecule at 3606 and 1576 cm^{-1}, respectively (Figure 3). The sharp stretching band near 3600 cm^{-1} indicates an unbonded hydroxyl group, which is consistent with the result from X-ray structure analysis. The presence of a lattice water molecule is also confirmed by solid-state NMR spectroscopy (vide infra).

Figure 4 shows a view of the structure along the *c*-axis. The structure can be described as consisting of infinite spiral chains of corner-sharing SiO_4 tetrahedra running parallel to the *c*-axis with a period of four tetrahedra. Each chain spirals around the 4_1-axis and is linked to four neighboring chains

(19) Brown, I. D.; Altermatt, D. *Acta Crystallogr.* **1985**, *B41*, 244.

(20) Donnay, G.; Allmann, R. *Am. Mineral.* **1970**, *55*, 1003.

(21) Brown, G. E.; Gibbs, G. V. *Am. Mineral.* **1969**, *54*, 1528.

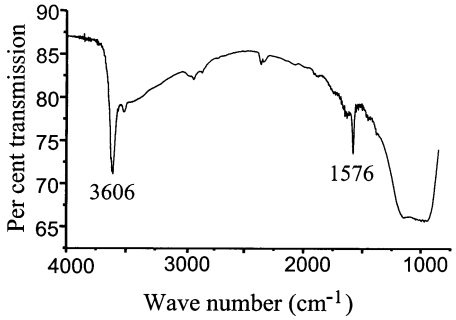

Figure 3. Infrared spectrum of $Rb_2(VO)(Si_4O_{10})\cdot xH_2O$.

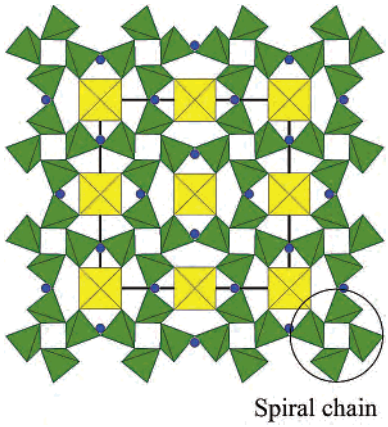

Figure 4. Structure of $Rb_2(VO)(Si_4O_{10})\cdot xH_2O$ viewed along the *c* axis. The yellow and green polyhedra are VO_5 square pyramids and SiO_4 tetrahedra, respectively. Blue circles are rubidium atoms. The partially occupied lattice water sites are not shown.

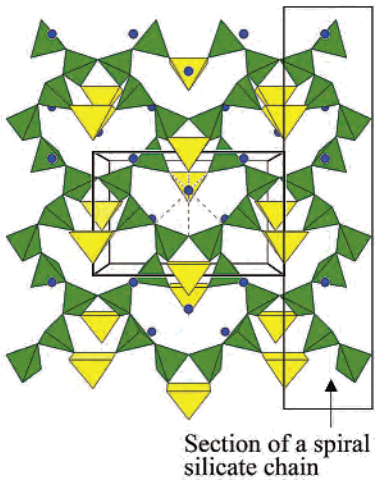

Figure 5. Perspective view of the $Rb_2(VO)(Si_4O_{10})\cdot xH_2O$ structure along the *a* axis. The dashed lines represent the Rb−O bonds.

via corner sharing to form a 3-D silicate framework which delimits channels to accommodate the vanadium atoms. The VO_5 square pyramid shares four of its vertexes with four silicate chains with the vanadyl group being unshared and directed along the *c*-axis. The Rb^+ ions are located in the cavities within the silicate framework and are coordinated to five silicate oxygen atoms and one vanadyl oxygen atom (Figure 5). The coordination polyhedron of Rb approximates a strongly distorted octahedron.

Figure 6 shows the inverse magnetic susceptibility of $Rb_2(VO)(Si_4O_{10})\cdot xH_2O$ plotted as a function of temperature. The

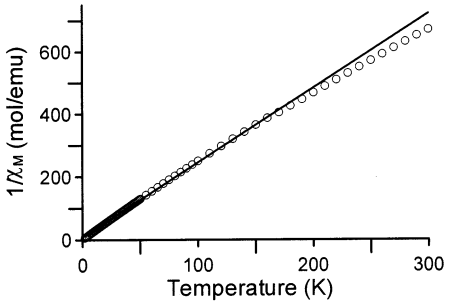

Figure 6. $1/\chi_M$ versus *T* for a powder sample of $Rb_2(VO)(Si_4O_{10})\cdot xH_2O$.

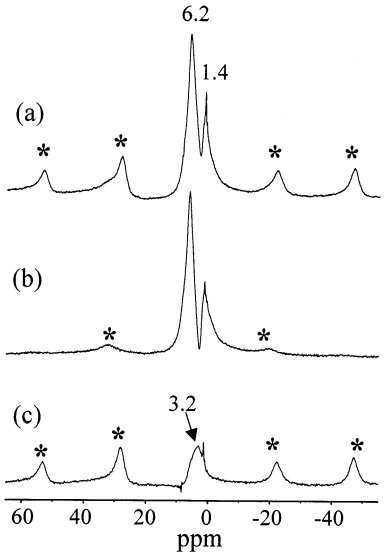

Figure 7. ^1H MAS NMR spectra of (a) as-synthesized $Rb_2(VO)(Si_4O_{10})\cdot xH_2O$ and (b) background signals from the probe and rotor under the same experimental conditions as (a), collected at a spinning speed of 10 kHz. The signal at 3.2 ppm, shown in the difference spectrum (c), is due to the lattice water molecule. Asterisks denote spinning sidebands.

data curves downward at higher temperatures, which could arise from the contribution of temperature independent paramagnetism. The data from 2 to 200 K were described well by a Curie−Weiss equation: $\chi_M = C/(T - \theta)$ where $C = 0.419$ cm^3·K/mol and $\theta = -2.95$ K. From the equation $C = N\mu_{eff}/3k_B$, one obtains the effective magnetic moment μ_{eff} per metal atom = 1.83, which confirms the presence of vanadium(IV).

^1H MAS NMR was employed to confirm the presence of trace amount of water molecules inside the framework of $Rb_2(VO)(Si_4O_{10})\cdot xH_2O$. Figure 7a shows the ^1H MAS NMR spectrum of $Rb_2(VO)(Si_4O_{10})\cdot xH_2O$. The spectrum consists of two resonances at 6.2 and 1.4 ppm, respectively. These signals are the background signals from the probe head and rotor because these resonances are also present when the spectrum is acquired under identical conditions without the sample (see Figure 7b). There appears to be another isotropic resonance at about 3 ppm in Figure 6a, which is obscured by the background signals but gives rise to the first-order spinning sidebands at 28.0 and −22.4 ppm. Figure 7c was obtained by subtracting Figure 7b from Figure 7a. The major contribution to the intensity of the sideband is from homonuclear $^1H-^1H$ dipolar coupling between the two hydrogen atoms in a water molecule. This suggests that the water molecule is not free to undergo translational motion and

molecular reorientations in the time scale of the $^1H-^1H$ dipolar coupling. We therefore ascribe the resonance at 3.2 ppm to the lattice water molecule rather than a moist sample.

The reason the spinning sidebands are such intense lines as compared with the central line is explained as follows. Depending on the mobility of the water molecule in the lattice, the relative intensities between the central line and the spinning sidebands may change, though the same spinning speed is employed. For instance, if the water molecule in the lattice is rigid, its ^1H NMR spectrum should in theory look like "Pake doublet",[22] in which the intensity of the central line is much smaller than those of the spinning sidebands. On the other hand, the central line dominates if the water molecule is very mobile. In our case, the water molecule is quite rigid but still has certain degrees of motional freedom. This motion scales down the intensities of spinning sidebands in the "Pake doublet" and results in an increase in intensity of the central line. This is the reason the first-order spinning sidebands are almost as intense as the central line as seen in Figure 4c, though a high spinning speed of 10 kHz was used.

Although $Rb_2(VO)(Si_4O_{10})$, the two polymorphs of the mineral $Ca(VO)(Si_4O_{10})\cdot 4H_2O$, and $K_2(VO)(Si_4O_{10})\cdot H_2O$ have the same framework stoichiometry, they adopt considerably different structures. Both $Ca(VO)(Si_4O_{10})\cdot 4H_2O$ and $K_2(VO)(Si_4O_{10})\cdot H_2O$ consist of silicate single layers which are linked by VO_5 square pyramids into three-dimensional frameworks containing channels that house metal cations and water molecules. The silicate layer in cavansite comprises 4-rings and 8-rings, but in pentagonite, the layer is entirely made up of 6-rings. The silicate layer of $K_2(VO)(Si_4O_{10})\cdot H_2O$ also comprises 6-rings, but the orientation of tetrahedra is different from that in pentagonite. In contrast, the framework of $Rb_2(VO)(Si_4O_{10})\cdot xH_2O$ is based on a building principle different from those of the above three layer-silicate structure types. The structure of $Rb_2(VO)(Si_4O_{10})\cdot xH_2O$ is new and is the first example of transition metal silicate obtained hydrothermally under high temperature and high pressure. Additional members belonging to this large family have been synthesized and will be reported elsewhere.

Acknowledgment. We thank the National Science Council for support, Ms. F.-L. Liao and Professor S. -L. Wang at National Tsing Hua University for X-ray intensity data collection, and Ms. R.-R. Wu at National Cheng Kung University for NMR measurements.

Supporting Information Available: Crystallographic data, in CIF format. This material is available free of charge via the Internet at http://pubs.acs.org.

IC020187Q

(22) Pake, G. E. *J. Chem. Phys.* **1948**, *16*, 327.